Determination of the background neutral density from passive Balmer alpha CX emission at the ASDEX Upgrade tokamak

A. Jansen van Vuuren[1], K. Bogar[2], D.J. Cruz-Zabala[1], M. Cavedon[3], P. Cano-Megias[4], A. Kappatou[3], R. Dux[3], P.A. Schneider[3], E. Viezzer[1], T. Nishizawa[3], M. Garcia-Munoz[1] and the ASDEX Upgrade Team[3]

[1] *Dept. of Atomic, Molecular and Nuclear Physics, University of Seville, Spain*

[2] *Institute of Plasma Physics of the CAS, CZ-18200 Prague, Czech Republic*

[3] *Max-Plank-Institut für Plasmaphysik, D-85748 Garching, Germany*

[4] *Dept. of Energy Engineering, University of Seville, Spain*

Introduction

Knowledge of the background neutral density is useful for detailed plasma transport studies. This is because background neutrals act both as a particle source via ionisation processes and a sink via charge exchange (CX) reactions with plasma particles. Recently developed techniques have demonstrated that 1D neutral deuterium density profiles can be inferred by analysing the contribution of CX reactions to the measured neon emission [1] as well as directly from neutral particle analyser (NPA) measurements [2]. However, additional techniques that rely on independent measurements can help to further constrain the inferred neutral density.

In this work, the passive Balmer alpha emission is used to obtain information on the density and distribution of background neutrals. This is possible as information on the neutral density along a given line of sight (LOS) is contained in the measured intensity. Furthermore, the spatial information on the distribution of the neutrals along a LOS is contained in the spectral shape of the emission. This is due to the Doppler shift produced by neutrals that have undergone CX reactions and therefore have velocity distributions determined by the local ion temperature. Given information on the plasma kinetic profiles, 1D neutral density profiles can be inferred by inversion techniques as have been demonstrated on fusion devices such as the LHD stellarator [3].

Experimental setup

Measurements of the passive Balmer alpha emission were performed with two dedicated spectroscopic systems recently installed on the ASDEX Upgrade tokamak [4]. The systems were connected to in vessel optics that view the high-field-side (HFS) [5] and low-field-side (LFS) midplane regions, respectively. Figs. 1a and b illustrate the viewing geometry of two LOS from the respective optical heads as well as that of the passive NPA diagnostic. The contour maps indicate the expected birth distribution, in logarithmic scale, of neutrals resulting from CX reactions that emit Balmer emission measured by either LOS. The distributions have been calculated using the FIDASIM code [6] using a 1D neutral density profile calculated by the 1D neutral transport code KN1D [7]. As can be seen in fig. 1a and b the CX neutrals are able to travel a considerable distance before crossing a LOS and emitting a photon. However, due to the large density of background neutrals in the scrape-off layer (SOL) the majority of emitting neutrals originate near the separatrix as can be seen in fig. 1c.

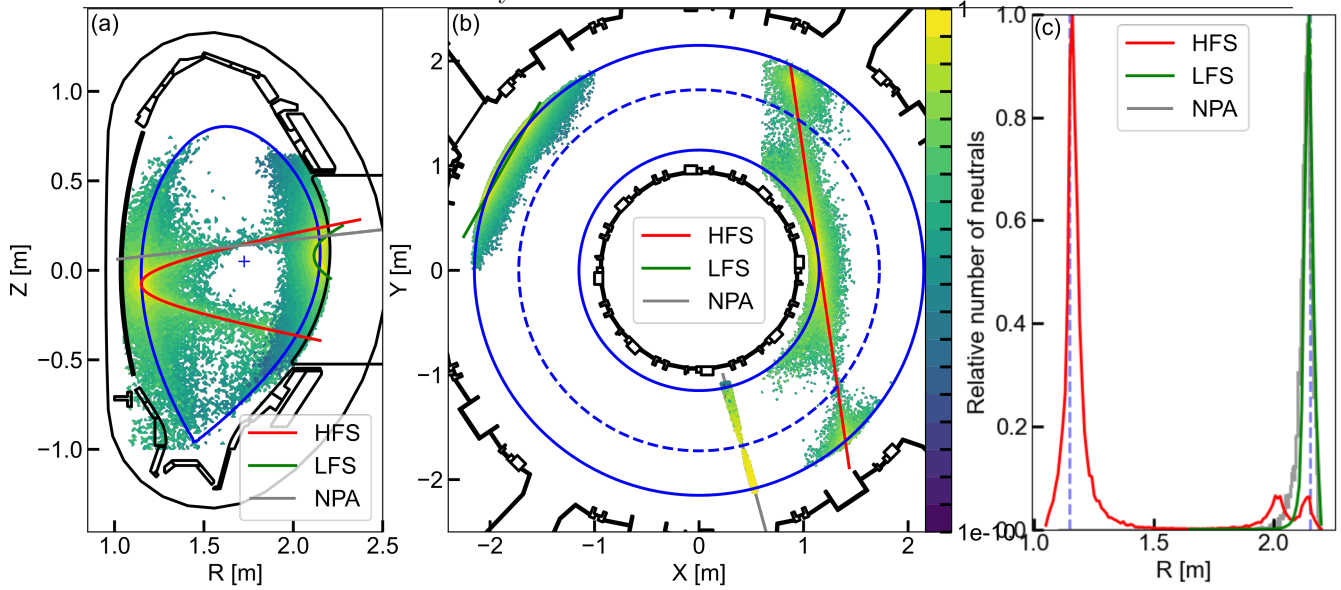

Figure 1: (a) Poloidal projection and (b) top down view of the FIDASIM predicted spatial distribution of neutrals that have undergone CX reactions and emit Balmer photons collected by one of the two LOS. (c) The radial distribution of the neutrals observed by both views as well as the NPA diagnostic.

Analysis methodology

A forward modelling approach is followed to determine the 1D neutral density profiles that produce synthetic spectra that best agree with measurements. Here, the model developed in [8, 9] is used as it has the advantage of being computationally inexpensive which allows for direct fitting of the measured spectra. Importantly, the model considers that neutrals may have originated from regions not directly in view of a given LOS. A brief overview of the model is presented here, closely following the description in [9]. It is important to note that the model assumes the emission and hence, neutral density is toroidally and poloidally symmetric. Furthermore, the emission is assumed to result from two populations of excited background neutrals. The first population being atomic neutrals formed during the dissociation of molecular deuterium which have energies of a few eV, here referred to as cold neutrals. The second population is formed by neutrals that result from CX reactions with thermal plasma ions and hence have energies determined by the plasma ion temperature.

The cold emission contribution is modelled by combining ten Gaussians with temperatures $T_{cold} = 1$ to 10 eV:

$$I_{cold}(\lambda) = \sum_{i=1}^{10} c_i \exp\left[-\frac{\Delta\lambda^2}{w_i^2}\right] \quad , w_i = \lambda_0 \sqrt{\frac{2kT_{cold,i}}{Mc^2}} \tag{1}$$

Where λ_0 =656.1 nm, M is the mass of deuterium and c is the speed of light. Here, the individual intensity c_i is used as the fit parameter. The CX emission contribution is modelled by dividing the plasma minor radius r in N (up to 20) sections and summing the emission from each section, labelled r_i (of length $\Delta L(r_i)$). Similar to the cold contribution, the spectral shape in terms of wavelength (λ) is determined by a Gaussian, however

in this case with a width determined by the local ion temperature $T_{D^+}(r_i)$:

$$I_{CX}(\lambda) = \sum_{i=1}^{N} n_e(r_i) n_0(r_i) \Delta L(r_i) PEC_{3\to 2} \times \frac{1}{\sqrt{\pi} w_{CX}(r_i)} \exp\left[-\left(\frac{\Delta\lambda}{w_{CX}(r_i)} \right)^2 \right] \quad , w_{CX}(r) = \lambda_0 \sqrt{\frac{2kT_{D^+}(r)}{Mc^2}} \tag{2}$$

Where $PEC_{3\to 2}$ is the Balmer alpha photon emission coefficient obtained from the ADAS open database. This formulation allows $n_0(r)$ to be treated as a parameter given that the plasma density $n_e(r)$ and ion temperature $T_{D^+}(r)$ are known and can be determined directly by fitting I_{CX} to the measured spectra. However, the problem is ill-posed and regularisation is required to obtain physically reasonable n_0 profiles. In this work a well-behaved parametric function for n_0 is used instead. The function expresses n_0 in terms of the normalised radius ρ using 5 parameters as described in [2].

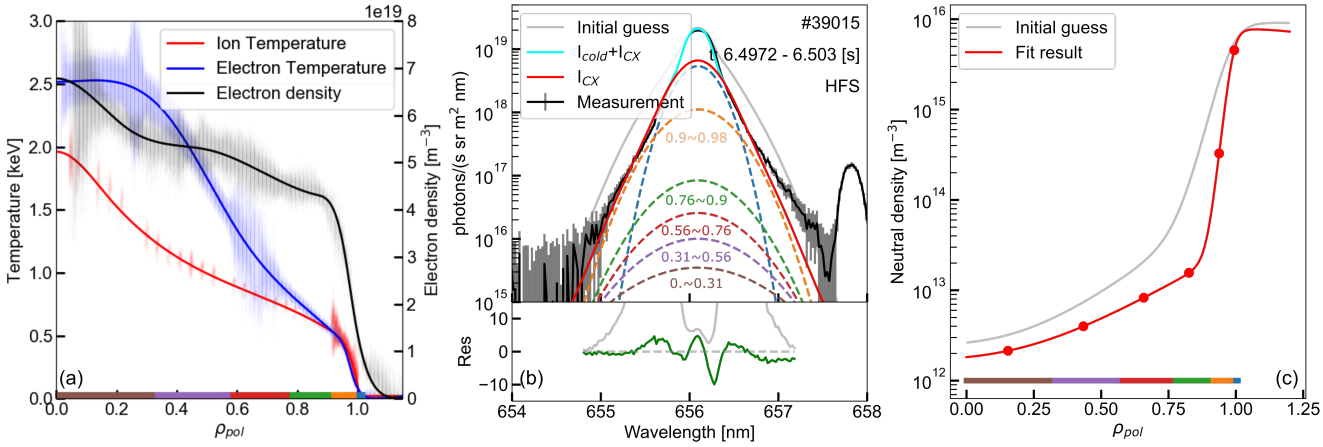

Figure 2: (a) Example input plasma profiles. (b) Fit to measured spectra with the initial guess in grey and the various contributions to I_{CX} plotted with dashed lines. (c) Initial guess and output neutral density profiles.

In order to forward model the Balmer emission for a given discharge and time point input profiles including the electron density, temperature and ion temperature are prepared as illustrated in figure 2a. Here it is assumed that the deuterium ion temperature is equal to the impurity ion temperature. The profiles are divided in N (in this example 6) sections indicated by the coloured blocks above the radial axis, to calculate the contribution of neutrals originating from these regions. Note, the sections are smallest at the separatrix where the profile gradients are steepest and increase in size towards the core as determined by the expression $\rho_i = 1.2 \times (1 - i/N)^3$. A fit routine is used to vary the parameters of the $n_0(\rho)$ function and obtain a best fit of I_{cold}+ I_{CX} to the measured spectrum as shown in fig 2b. Here I_{cold}+ I_{CX} is plotted in cyan, while the individual contributions to I_{CX} from each region are plotted with dashed lines in the corresponding colour. Fig. 2c shows the n_0 profiles corresponding to the initial guess of fit parameters in grey and the resulting best fit parameters in red.

Results and discussion

The analyses method has been applied to obtain neutral densities from measurements of the HFS and LFS Balmer emission for discharge #39015 (see fig. 3). The fit to the HFS spectrum is shown in fig. 3a and is compared to a FIDASIM calculated spectrum using the fitted neutral density (in magenta) and a KN1D calculated neutral density profile (in blue). Good agreement between the spectrum fit and FIDASIM

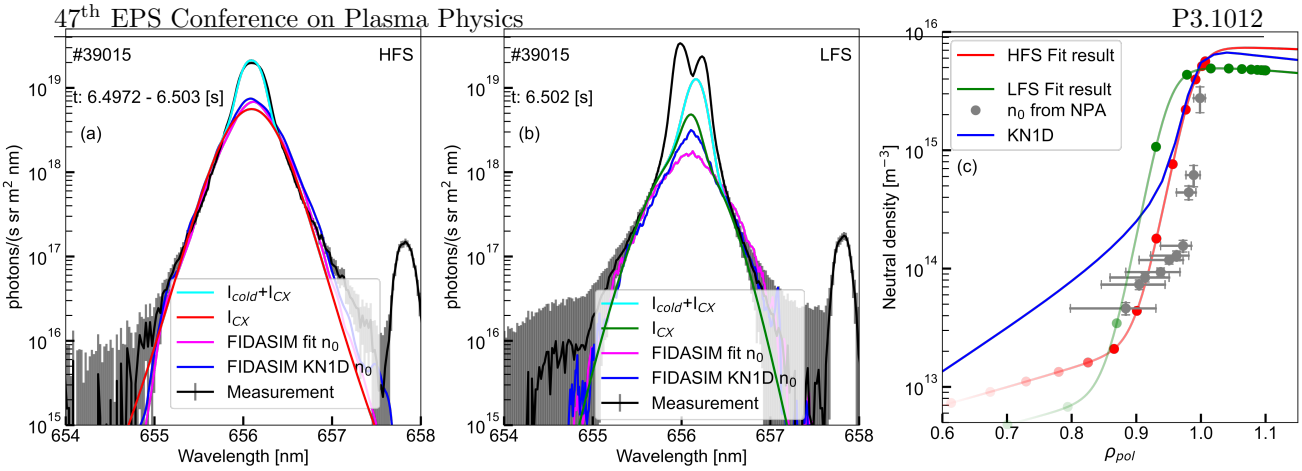

Figure 3: (a) HFS and (b) LFS measured spectra (black) including fit and FIDASIM forward modelled results. (c) Calculated neutral density profiles.

is observed suggesting that the analysis method models well the effect of distant neutrals reaching the LOS. Fig. 3b shows the fit to the LFS measured spectra. Here again a good agreement between the fit and FIDASIM calculated spectrum is found, however it should be noted that the fit does not yet produce a good match to the cold emission and improvements to the fit are currently ongoing. Finally, fig. 3c compares the neutral density profiles obtained from the fits to the spectra. These profiles are compared to a KN1D calculated neutral density profile as well as the neutral density values obtained from NPA measurements. As can be seen the neutral density is calculated to be larger in the HFS SOL compared to the LFS, while the reverse is observed in the steep gradient region. The HFS profile agrees well with the KN1D modelled density in the SOL and high gradient regions however a large difference is observed further inside. However, since the measured emission largely originates from the region around the separatrix the uncertainty in the fitted neutral density profiles in the core region is expected to be large. Lastly, comparing the neutral density values calculated from NPA measurements show a reasonably good agreement with the HFS density profile, while the LFS neutral density is calculated to be larger. This may be explained by a strong toroidal asymmetry in the background neutral density as the NPA and LFS LOS view toroidally separate regions.

Acknowledgements

This work has been carried out within the framework of the EUROfusion Consortium and has received funding from the Euratom research and training programme 2014-2018 and 2019-2020 under grant agreement No 633053. The views and opinions expressed herein do not necessarily reflect those of the European Commission.

References

[1] R. Dux et al, Nucl. Fusion **60**, 126039 (2020)

[2] K. Bogar et al, Nucl. Fusion **61**, 036001 (2021)

[3] M. Goto et al, Nucl. Fusion **51**, 023005 (2011)

[4] A. Jansen van Vuuren et al, Rev. Sci. Instrum. **90**, 103501 (2019)

[5] D.J. Cruz-Zabala et al, JINST **14** C11006 (2019)

[6] B. Geiger et al, Plasma Phys. Control. Fusion **62** 105008 (2020)

[7] B. LaBombard, Massachusetts Institute of Technology, Plasma Science and Fusion Center Research Report PSFC-RR-01-3 (2001)

[8] K. Fujii et al, Rev. Sci. Instrum. **85**, 023502 (2011)

[9] K. Fujii et al, Nucl. Fusion **55**, 063029 (2015)